

**Quantifying the role of internal climate variability
in future climate trends**

David W. J. Thompson^{1, 2}, Elizabeth A. Barnes², Clara Deser³,
William E. Foust², Adam S. Phillips³

Submitted to Journal of Climate

December 2014

¹ Corresponding author. Email: davet@atmos.colostate.edu.

² Department of Atmospheric Science, Colorado State University, Fort Collins, CO. USA

³ National Center for Atmospheric Research, Boulder CO. USA

1 **Abstract**

2 Internal variability in the climate system gives rise to large uncertainty in
3 projections of future climate. The uncertainty in future climate due to internal climate
4 variability can be estimated from large ensembles of climate change simulations in
5 which the experiment set-up is the same from one ensemble member to the next but for
6 small perturbations in the initial atmospheric state. However, large ensembles are
7 invariably computationally expensive and susceptible to model bias.

8 Here we outline an alternative approach for assessing the role of internal
9 variability in future climate based on a simple analytic model and the statistics of the
10 unforced climate variability. The model is derived from the standard error of the
11 regression and assumes that the statistics of the internal variability are roughly
12 Gaussian and stationary in time. When applied to the statistics of an unforced control
13 simulation, the model provides a remarkably robust estimate of the uncertainty in
14 future climate indicated by a large ensemble of climate change simulations.

15 It is argued that the uncertainty in future climate trends due to internal
16 variability can be robustly estimated from the statistics of the observed variability.

17

1 **Introduction**

2 The signature of anthropogenic forcing in climate change has and will be
3 superposed on internal climate variability due to a variety of physical processes (e.g.,
4 Hawkins and Sutton 2009, 2011; Deser et al. 2012a, 2012b; Wallace et al. 2013; Kirtman
5 and Power et al. 2013; Collins and Knutti et al. 2013; Knutson et al. 2013; Bindoff and
6 Stott et al. 2013). At most terrestrial locations, a large component of the internal
7 variability in surface climate change arises from variations in the atmospheric
8 circulation (Wallace et al. 1995, 2012, 2013; Deser et al. 2014). On regional spatial
9 scales, the internal variability can overwhelm the signature of anthropogenic forcing not
10 only on year-to-year timescales, but on multidecadal timescales as well (Hawkins and
11 Sutton 2009; Deser et al. 2012a, 2012b; IPCC 2014). Understanding and predicting the
12 contribution of internal variability to long-term trends in climate is essential for both
13 the adaption to and mitigation of climate change (IPCC 2014).

14 What is the most robust way to estimate the role of internal variability in future
15 climate trends? One approach is to generate a large ensemble of climate change
16 simulations in which the individual ensemble members are from the same climate
17 model and subject to the same external forcing, but are initiated with slightly different
18 atmospheric initial conditions. For example, the National Center for Atmospheric
19 Research (NCAR) CCSM3 Large Ensemble Project includes 40 climate change
20 simulations run with the same coupled atmosphere-ocean-sea ice-land model (the
21 NCAR Community Climate System Model 3; CCSM3) and forced with identical
22 projected changes in greenhouse gases and ozone from 2000-2061 (the SRES A1B
23 Scenario). Since the model and forcing are the same in all ensemble members, the
24 differences in climate trends from one ensemble member to the next derive entirely

1 from the unforced (i.e., internal) variability in the model.

2 Analyses of the spread in the trends in the NCAR 40-member ensemble make
3 clear the pronounced role of internal climate variability in projections of regional
4 climate change (Deser et al. 2012a, 2012b). For example, the left panels in Figure 1 show
5 the standard deviations of the 50-year (2011-2061) trends in October-March mean near-
6 surface air temperature and precipitation calculated over all ensemble members (i.e.,
7 the results indicate the spread in the trends from one ensemble member to the next).
8 The right panels indicate time series of October-March mean surface air temperature
9 and precipitation for all 40 ensemble members at two sample locations. As noted in
10 Deser et al. (2012a), internal variability in the CCSM3 gives rise to temperature trend
11 standard deviations that exceed 1 K/50 years over much of the Northern Hemisphere
12 and precipitation trend standard deviations that exceed 0.5 mm/day/50 years over
13 much of the tropics. Since the spreads in the trends indicated in Fig. 1 arise entirely
14 from stochastic variability in the CCSM3, they may be viewed as the irreducible
15 component of uncertainty in climate change projections.

16 The purpose of this study is to develop a simple analytic model for estimating the
17 uncertainty in projections of future climate trends due to internal climate variability, as
18 exemplified in Fig. 1. The model is derived from the standard error of the regression and
19 is based on two statistics of the unforced climate variability: the standard deviation and
20 autocorrelation. The analytic model is developed in Section 2. It is tested against the
21 NCAR 40-member ensemble in Section 3 and applied to observations in Section 4.
22 Implications are discussed in Section 5.

23

2. A simple analytic model of the role of internal variability in future climate trends

Consider a time series $x(t)$ with mean zero and a linear least-squares trend b . The confidence interval (CI) on the trend in $x(t)$ is expressed as:

$$CI = b \pm e$$

where e is the margin of error for the trend. The trend, its confidence interval and its margin of error are all expressed in units $\Delta x / (n_t \Delta t)$, where n_t is the number of time steps and Δt is the time step. For example, if $x(t)$ corresponds to 50 years of wintertime mean temperature data, then $n_t = 50$, $\Delta t = 1$ year, and the temperature trend in $x(t)$ is expressed in units degrees Celsius/50 years.

If the distribution of the deviations in $x(t)$ about its linear trend (i.e., the residuals of the regression) is Gaussian, then the margin of error for the trend in $x(t)$ is:

$$1) \quad e = t_c s_b$$

where t_c is the t -statistic corresponding to the desired confidence interval and

$$2) \quad s_b = \frac{n_t s_e}{\sqrt{\sum_{i=1}^{n_t} (i - \bar{i})^2}}$$

1 is the standard error of the trend. In Eq. 2, i denotes time, s_e is the standard error of
 2 $x(t)$ about its linear trend, and the factor n_t is included so that the standard error is
 3 given in units $\Delta x / (n_t \Delta t)$. Equations 1 and 2 are widely used to assess the significance of
 4 a trend in climate science (Wilks 1995; von Storch and Zwiers 1999; Santer et al. 2000).

5 The standard deviation of the time axis (the denominator in Eq. 2) can be
 6 expanded as a function of n_t , since the time axis corresponds to a series of consecutive
 7 integers. Using two formulae for consecutive integers:

$$9 \quad \sum_{i=1}^{n_t} i = \frac{n_t(n_t+1)}{2} \quad \text{and} \quad \sum_{i=1}^{n_t} i^2 = \frac{n_t(n_t+1)(2n_t+1)}{6}$$

10
 11 it follows that:

$$13 \quad \bar{i} = \frac{1}{n_t} \sum_{i=1}^{n_t} i = \frac{(n_t+1)}{2}$$

14
 15 and:

$$17 \quad \begin{aligned} \sum_{i=1}^{n_t} (i - \bar{i})^2 &= \sum_{i=1}^{n_t} i^2 - \sum_{i=1}^{n_t} 2i \cdot \bar{i} + \sum_{i=1}^{n_t} \bar{i}^2 \\ &= \sum_{i=1}^{n_t} i^2 - (n_t+1) \sum_{i=1}^{n_t} i + \sum_{i=1}^{n_t} \left(\frac{n_t+1}{2} \right)^2 \\ &= \frac{n_t(n_t+1)(2n_t+1)}{6} - \frac{n_t(n_t+1)^2}{2} + \frac{n_t(n_t+1)^2}{4} \\ &= \frac{n_t^3 - n_t}{12} \end{aligned}$$

1
2
3
4
5
6
7
8
9
10
11
12
13
14
15
16
17
18
19
20
21

Thus, the contribution of the time axis to Eq. 2 can be written as:

$$3) \quad g(n_t) \equiv \frac{1}{\sqrt{\sum_{i=1}^{n_t} (i - \bar{i})^2}} = \sqrt{\frac{12}{n_t^3 - n_t}}$$

Note that the units on $g(n_t)$ are $1/\Delta t$.

Regarding the standard error of $x(t)$ about its linear trend (s_e in Eq. 2): If the residuals (the values of $x(t)$ about its linear trend) are *not* serially correlated (e.g., the lag-one autocorrelation of the detrended $x(t)$ time series is zero), then s_e is equal to the standard deviation of the detrended $x(t)$ time series:

$$4) \quad s_e = \sigma$$

where

$$5) \quad \sigma \equiv \sqrt{\frac{1}{n_t - 2} \sum_{i=1}^{n_t} [x(i) - bi]^2} .$$

In the context of climate change, σ corresponds to the standard deviation of the internal (unforced) variability.

If the detrended $x(t)$ time series is serially correlated, then s_e must include a scaling factor that accounts for the bias in the sample standard deviation introduced by

1 persistence in the time series (Mitchell et al. 1966; Wilks 1995; von Storch and Zwiers
 2 1999; Santer et al. 2000). A simple and commonly used method for accounting for the
 3 bias in the sample standard deviation is to substitute an effective sample size n_{eff} for the
 4 sample size n_t in the denominator of Eq. 5. If $x(t)$ is well-modeled as Gaussian red noise
 5 (and thus its autocorrelation function decays exponentially with lag), then n_{eff} can be
 6 approximated as (Mitchell et al. 1966; Santer et al. 2000):

$$8 \quad n_{eff} \sim n_t \left(\frac{1-r_1}{1+r_1} \right)$$

9
 10 Substituting the above for n_t in the denominator of Eq. 5 yields:

$$11 \quad 6) \quad s_e = \sigma \gamma(n_t, r_1)$$

12
 13 where

$$14 \quad 7) \quad \gamma(n_t, r_1) \equiv \left(\frac{[n_t - 2]}{\left[n_t \left(\frac{1-r_1}{1+r_1} \right) - 2 \right]} \right)^{1/2}$$

15
 16
 17
 18 is the scaling factor and r_1 is the lag-one autocorrelation of the residuals (the detrended
 19 $x(t)$ time series).

1 Substituting Eqs. 2, 3, and 6 into Eq. 1 yields the following expression for the
2 margin of error for a trend in $x(t)$ in units $\Delta x / (n_t \Delta t)$:

3
4 8) $e = t_c \cdot n_t \cdot \sigma \cdot \gamma(n_t, r_1) \cdot g(n_t)$

5
6 Equation 8 provides a simple analytic model for the margin of error for a trend in
7 a Gaussian red noise process. It makes clear that the margin of error is a function of two
8 statistics of the internal variability, both of which we assume are stationary in time:

- 9 1) the standard deviation of the internal (unforced) variability, σ ; and
10 2) the lag-one autocorrelation of the internal (unforced) variability, r_1 .

11 The ratio $\frac{e}{\sigma}$ corresponds to the amplitude of the trend required to exceed the
12 desired confidence level in units of the standard deviation of the internal variability. For
13 example, if $\frac{e}{\sigma} = 2$, then the trend must be twice as large as the internal (unforced)
14 variability to exceed its margin of error. Figure 2 shows solutions for $\frac{e}{\sigma}$ calculated from
15 Eq. 8 for the two-tailed 95% confidence level as a function of trend length (n_t , abscissa)
16 and lag-one autocorrelation (r_1 , ordinate). The required trend amplitude increases
17 rapidly as the length of the trend decreases and/or the autocorrelation increases. If a
18 time series is 40 time steps in length and has autocorrelation $r_1 = 0.45$, then the trend in
19 the time series must be twice as large as the standard deviation of the internal variability
20 to exceed the 95% confidence level. If the autocorrelation increases to ~ 0.65 , then the
21 trend must be \sim three times as large as the internal variability.

1 In the case where the trend length is at least ~ 20 timesteps ($n_t > \sim 20$) and the
 2 detrended $x(t)$ time series is not serially correlated ($r_1 \sim 0$), then the 95% margin of error
 3 for a trend simplifies to:

$$4$$

$$5 \quad 9) \quad e_{95\%} \sim \sigma \left\{ \frac{48}{n_t} \right\}^{1/2} \quad (\text{for } n_t > \sim 20 \text{ and } r_1 \sim 0)$$

6

7 where $e_{95\%}$ is in units $\Delta x / (n_t \Delta t)$ and we have made the following simplifications: 1)

$$8 \quad g(n_t) \sim \left(\frac{12}{n_t^3} \right)^{1/2} \quad \text{for } n_t > \sim 20 ; 2) \text{ the two-tailed 95\% } t\text{-statistic is } \sim 2 \text{ for } n_t > \sim 20 \text{ (if the}$$

9 sign of the trend is expected *a priori* then a one-tailed t -statistic is justified); and 3)

$$10 \quad \gamma \sim 1 \text{ for } r_1 \sim 0 .$$

11 Equation 9 holds for any physical process that is roughly Gaussian and is not
 12 serially correlated including, for example, seasonal-mean surface temperature and
 13 precipitation at most terrestrial locations. It makes clear the linear relationship between
 14 the standard deviation of the internal variability and the margins of error for climate
 15 trends due to the internal variability.

16 In the case where the trend length is 50 time steps, Eq. 9 further simplifies to:

$$17$$

$$18 \quad 10) \quad e_{95\%} \sim \sigma \quad (\text{for } n_t = 50 \text{ and } r_1 \sim 0)$$

19

20 Hence, for any Gaussian physical process that is not serially correlated from one year to
 21 the next, the 95% margin of error for the 50 year trend is roughly equal to the

1 interannual standard deviation. For example, if the interannual standard deviation is 2
2 degrees Celsius, then the two-tailed 95% confidence interval on the 50 year trend in
3 surface temperature is roughly ± 2 degrees Celsius/50 yrs.

4 5 **3. Testing the analytic model in a large ensemble of climate change** 6 **simulations**

7 How well does the analytic model predict the uncertainty in future climate
8 trends? The utility of the analytic model is tested by comparing: 1) the margins of error
9 in trends calculated from a large ensemble of climate change simulations run on a
10 coupled global climate model (the *actual* margins of error); with 2) the margins of error
11 predicted by applying the analytic model to the statistics of the internal variability of the
12 same coupled global climate model (the *predicted* margins of error). As discussed below,
13 the internal variability of the coupled global climate model is estimated from a long
14 control simulation with fixed anthropogenic forcing.

15 The *actual* margins of error are derived from 50-year trends in boreal wintertime
16 (October-March) and summertime (April-September) mean near-surface air
17 temperature and precipitation from the NCAR 40-member ensemble of climate change
18 simulations. The NCAR 40-member ensemble is described in detail in Deser et al.
19 2012a. Briefly, the simulations were run with a fully coupled ocean/land/atmosphere
20 global climate model on a 2.8 x 2.8 degree latitude/longitude grid (the NCAR
21 Community Climate System Model Version 3; CCSM3) and forced with the Special
22 Report on Emissions Scenarios (SRES) A1B scenario. The ensemble members differ only
23 in their initial atmospheric conditions. The *predicted* margins of error are derived from
24 a 1000 year-long control simulation run on the NCAR CCSM3 in which greenhouse

1 gases are held fixed at 1990 levels. In the analyses shown here, the climate change
2 simulations are examined from 2011-2061 and the control simulation is examined for
3 the last 500 years of the integration. Seasonal-mean surface air temperature and
4 precipitation do not exhibit notable memory from one year to the next at virtually all
5 terrestrial locations in the control run (bottom rows in Appendix Figures A1-A2). Hence
6 the predicted 95% margins of error for the 50-year trends are estimated as the
7 interannual standard deviations in the control run (Eq. 10).

8 Figure 3a shows the ensemble-mean 50-year trends in surface air temperature
9 from 2011-2061 averaged over all 40 members in the CCSM3 large ensemble. The
10 ensemble-mean trends have been discussed in previous work (Deser et al. 2012a) and
11 are shown here to provide context for the amplitude of the internal variability. The
12 warming during the first half of the 21st century is projected to be largest over the
13 Northern Hemisphere, where it exceeds ~ 3 K/50 years over much of northern North
14 America and Asia (Deser et al. 2012a; Kirtman and Power et al. 2013; Collins and Knutti
15 et al. 2013).

16 Figure 3b shows the *actual* two-tailed 95% margins of error for the 50-year
17 trends found by: 1) calculating the standard deviations of the trends derived from all 40
18 ensemble members and 2) multiplying the standard deviations by a factor of two (95%
19 of the normal distribution lies within \sim two standard deviations of the population
20 mean). Note that Fig. 3b is identical to Fig. 1a multiplied by a factor of two. The grey
21 bars in the surrounding panels indicate the histograms of the simulated trends at grid
22 boxes collocated with the indicated cities. The actual margins of error for the trends are
23 due entirely to the internal variability in the NCAR CCSM3, i.e., they are not due to
24 differences in the forcing or the model used in the simulations. As such, they provide a

1 quantitative estimate of the role of internal variability in future climate trends (Deser et
2 al. 2012a, 2012b). By construction, the means of the histograms are equal to the trends
3 in Fig. 3a and the standard deviations of the histograms are equal to 0.5 times the actual
4 margins of errors shown in Fig. 3b. At many terrestrial locations, the margins of error
5 due to internal variability are ~50% as large as the forced signal (compare Figs. 3a and
6 3b).

7 Figure 3c shows the *predicted* 95% margins of error for the 50-year trends found
8 by applying the analytic model to the statistics of the control simulation. That is: since
9 we are applying Eq. 10, the results simply show the interannual standard deviations
10 from the control simulation. Stippling indicates regions where the predicted margins fall
11 within the 95% confidence range of the actual margins. The confidence ranges on the
12 actual margins are found by: 1) calculating the 95% confidence ranges on the
13 interannual standard deviations from the control simulation using the Chi-squared
14 distribution; 2) multiplying the resulting confidence ranges by a factor of 2 to convert
15 them to confidence ranges on the predicted margins of error. The blue probability
16 density functions in the surrounding panels show the corresponding predicted Gaussian
17 distributions of the trends at grid boxes collocated with the indicated cities, where 95%
18 of the distributions lies between $\pm e_{95\%}$.

19 Comparing Figs. 3b and 3c, it is clear that 1) the interannual standard deviations
20 in surface air temperature from the control run provide a remarkably accurate
21 prediction for 2) the margin of error on the trends in surface air temperature derived
22 from the large-ensemble of climate change simulations. Over much of the globe, the
23 predicted margins of error are statistically indistinct from the actual margins.

1 Figure 4 shows analogous results for October-March mean precipitation. The
2 ensemble-mean trends (Fig. 4a) are consistent with increases in precipitation in the
3 deep tropics and high northern latitudes juxtaposed against decreases in precipitation in
4 the subtropics (Kirtman and Power et al. 2013; Collins and Knutti et al. 2013; Held and
5 Soden 2006). As is the case for surface air temperature, the predicted margins of error
6 given by the interannual standard deviations from the control run provide a remarkably
7 accurate estimate of both the spatial pattern and amplitude of the actual margins of
8 error throughout much of the globe (compare Figs. 4b and 4c). The predicted margins of
9 error are within the 95% confidence range of the actual margins over most terrestrial
10 locations.

11 Results for the boreal summer season (April-September) are shown in Figures 5
12 and 6. In the case of precipitation (Fig. 6), the similarities between the predicted and
13 actual margins of error are comparable to those indicated in Fig. 4. In the case of surface
14 air temperature (Fig. 5), the predicted margins of error are within the 95% bounds of the
15 actual margins over most of the globe except for the high latitudes of Asia and North
16 America, where the predicted margins of error are ~50% less than those derived from
17 the CCSM3 large ensemble. The reasons for the differences between the predicted and
18 actual margins of error over Canada and Siberia during April-September are unclear.
19 They do not lie in a region of obvious changes in the interannual variance of surface air
20 temperature (Appendix Fig. A3, top right). Rather, the differences may simply reflect
21 sampling variability: As indicated in Fig. 7, the predicted and actual ranges of the trends
22 over the high latitudes of Asia and North America exhibit considerable overlap except
23 for a few ensemble members on the wings of the distributions.

24 As noted earlier, the analytic model is based on two primary assumptions. One, it

1 assumes that the internal variability is roughly Gaussian and is not dominated by, say,
2 bimodal or oscillatory behavior. The climate system exhibits various forms of quasi-
3 periodic variability other than the seasonal cycle, e.g., the Madden-Julian Oscillation
4 (Zhang 2005) and El-Nino/Southern Oscillation. But a substantial fraction of climate
5 variability is well-modeled as a Gaussian process, particularly at extratropical locations
6 (Hartmann and Lo 1998; Feldstein 2000; Newman et al. 2003) and on interannual
7 timescales. Two, it assumes that the standard deviation and autocorrelation of the
8 internal variability are stationary in time. There is evidence that the standard deviation
9 of surface air temperature will change over select locations in response to climate
10 change, with decreases in temperature variance over the high latitudes of the Northern
11 Hemisphere during winter (e.g., Gregory and Mitchell 1995; Screen 2014; Schneider et
12 al. 2015) and increases over various terrestrial regions in summer (Fischer and Schär
13 2009). The most noticeable changes in interannual variance in the NCAR CCSM3 large-
14 ensemble of climate change simulations are found over eastern Europe/western Russia,
15 where the standard deviations of surface air temperature decrease during the forcing
16 period (Appendix Fig. A3). But even in this region, the differences between the predicted
17 and actual margins of error are not statistically significant (Fig. 3c). As demonstrated in
18 Figs. 3-6, the analytic model provides a remarkably robust estimate of the uncertainty in
19 simulated climate change due to internal variability over the vast majority of the globe.

20

21 **4. Application to observations**

22 The results in the previous section indicate that the role of internal variability in a
23 large ensemble of climate change simulations can be quantified to a high degree of

1 accuracy from the statistics of the variability in an unforced control simulation. The
2 results highlight the importance of simulating correctly the internal variability in a
3 control simulation: If the standard deviation and/or autocorrelation of the simulated
4 internal variability are biased relative to the observations, then those biases will project
5 directly onto the uncertainty in simulations of climate change. Since model simulations
6 inevitably contain biases, the internal variability of the *real-world* is arguably best
7 estimated from the *real-world* itself, i.e., from observations.

8 The analytic model is applied to estimates of internal variability derived from two
9 observational data sources: 1) precipitation data from the Global Precipitation
10 Climatology Project (GPCP) Version 2.2 Combined Precipitation Data Set (Adler et al.
11 2003), and 2) surface air temperature data from the HadCRUT4 dataset (Kennedy et al.
12 2011; Osborn and Jones 2014). The precipitation data are analyzed on a 2.5x2.5 mesh
13 and were obtained from the NOAA Physical Sciences Division; the surface air
14 temperature data are analyzed on a 5x5 mesh and were obtained from the Climatic
15 Research Unit at the University of East Anglia.

16 The observed internal climate variability is assumed to be closely approximated
17 by the statistics of the detrended, seasonal-mean grid point values over the period 1979-
18 2013. In principle: 1) the anthropogenic forcing of the past few decades is not perfectly
19 linear; and 2) the amplitude of the internal variability on decadal timescales may be
20 underestimated in the relatively short 1979-2013 period. However, in practice: 1) the
21 statistics of the grid point surface air temperature and precipitation observations are
22 effectively identical whether the anthropogenic signal is modeled as a first order (linear
23 trend) or second order polynomial fit; and 2) variations on decadal timescales account

1 for a relatively small fraction of the total variance in surface air temperature and
2 precipitation on regional scales (not shown).

3 Figures 8 and 9 compare the 95% margins of error for the 50-year October-
4 March mean surface air temperature and precipitation trends derived from a) the
5 observations (top panels; solid distributions in surrounding panels) and b) the CCSM3
6 control simulation (bottom panels; dashed distributions). As is the case for the control
7 simulation output, observed October-March mean surface air temperature and
8 precipitation do not exhibit statistically significant memory from one year to the next at
9 virtually all terrestrial locations (Appendix Figs. A1 and A2, top rows). Hence, the
10 predicted 95% margins of error for the 50-year trends derived from the observations are
11 roughly equal to the standard deviations of the (detrended) October-March mean data
12 (Eq. 10). Note that the results in Figs. 8b and 9b are identical to those shown in Figs. 3c
13 and 4c, respectively, except that: 1) the stippling in Figs. 8b and 9b indicates regions
14 where the modeled and observed interannual variances are significantly *different* from
15 each other at the 95% confidence level (ratios $>1.5:1$ or $<1:1.5$ exceed the 95%
16 confidence level based on a test of the F-statistic assuming one degree of freedom per
17 year); and 2) the control simulation output used in Figs. 8 and 9 has been interpolated
18 to the same mesh as the observations before calculating the interannual standard
19 deviations (i.e., the temporal variance of area-mean surface air temperature and
20 precipitation generally decreases when averaged over successively larger spatial
21 regions). Results for April-September mean data are shown in Figures 10 and 11.

22 The margins of error predicted by the CCSM3 control simulation and
23 observations exhibit similar spatial patterns but have significantly different amplitudes
24 over large regions of the globe (stippling). For example, the control simulation exhibits

1 significantly different margins of error in surface air temperature over much of western
2 North America, southern Asia, and tropical South America and Africa (Fig. 8). It also
3 exhibits significantly different margins of error in precipitation over much of North
4 America, South America and eastern Asia (Fig. 9). The differences between the margins
5 of error predicted by the observed and control interannual standard deviations are
6 visually apparent at several of the indicated cities (probability distribution functions).
7 Comparable differences are found during the April-September season in both surface air
8 temperature and precipitation (Figs. 10 and 11).

9

10 **Concluding remarks**

11 The analytic model outlined here may be viewed as a “null hypothesis” for the
12 role of internal variability in future climate in *any* physical field that is well-modeled as
13 a Gaussian process. It thus provides a zeroth-order estimate of the uncertainty in future
14 trends in a host of physical fields averaged over a range of spatial scales including, for
15 example, precipitation averaged over a specific watershed, surface air temperature
16 averaged over a broad agricultural region, the atmospheric circulation at middle
17 latitudes, and global-mean temperature.

18 The model is based on two assumptions: 1) the internal variability is well-
19 modeled as Gaussian; and 2) the standard deviation and/or autocorrelation of the
20 internal climate variability do not change in response to anthropogenic forcing. The
21 robustness of the model to both assumptions is strongly supported by the close
22 similarities between: 1) the uncertainties in climate trends estimated by the statistics of
23 an unforced control simulation and 2) the uncertainties found in a large-ensemble of
24 climate change simulations over the next 50 years. The results imply that large-

1 ensembles provide little information on the role of internal variability in future climate
2 that can not be inferred from the standard deviation and autocorrelation of an unforced
3 control simulation.

4 Ensembles of climate change simulations with a single model are required to
5 estimate the amplitude of the model's forced signal in the presence of random internal
6 climate variability. But even in this case, the benefits of running large-ensembles are
7 strongly constrained by the central limit theorem, which dictates that the reduction in
8 the amplitude of the (random) internal variability in the ensemble-mean scales as $\frac{1}{\sqrt{N}}$
9 , where N is the number of ensemble members. Hence, the benefit of running additional
10 ensemble members rapidly drops beyond a relatively small number of runs. For
11 example, the amplitude of the internal variability in the climate model is reduced by
12 29% in the ensemble-mean when N is increased from one to two members, but by only
13 ~1.7% when N is increased from nine to ten members, and by only ~0.2 % when it is
14 increased from 39 to 40.

15 The results also make clear the direct relationship between 1) biases in the
16 variability and persistence of the climate in an unforced control simulation and 2) the
17 uncertainty in projections of future climate trends. In the case of wintertime-mean
18 surface air temperature or precipitation, the bias in the standard deviation of the
19 unforced variability scales linearly with the bias in the margin of error for the 50-year
20 trends (Eq. 10). To the extent that albeit imperfect observational records provide a more
21 realistic representation of the real-world than a climate model, it follows that the role of
22 internal variability in future climate trends is arguably best estimated not from a long

1 control simulation or a large-ensemble of climate change simulations, but from the
2 statistics of the observed climate.

3

4 **Acknowledgments**

5 We thank J. M. Wallace for insightful comments on the results. NCAR is
6 sponsored by the National Science Foundation. DWJT, EAB and WEF are supported by
7 the National Science Foundation Climate Dynamics program.

8

9

10

1 **References**

2 Adler, R.F., et al, 2003: The Version 2 Global Precipitation Climatology Project (GPCP)

3 Monthly Precipitation Analysis (1979-Present). *J. Hydrometeor.*, 4, 1147-1167.

4 Bindoff, N.L., P.A. Stott, et al., 2013: Detection and Attribution of Climate Change: from

5 Global to Regional. In: *Climate Change 2013: The Physical Science Basis.*

6 *Contribution of Working Group I to the Fifth Assessment Report of the IPCC*

7 [Stocker, T.F., et al. (eds.)]. Cambridge University Press, Cambridge, United

8 Kingdom and New York, NY, USA.

9 Collins, M., R. Knutti, et al., 2013: Long-term Climate Change: Projections,

10 Commitments and Irreversibility. In: *Climate Change 2013: The Physical Science*

11 *Basis. Contribution of Working Group I to the Fifth Assessment Report of the IPCC*

12 [Stocker, T.F., et al. (eds.)]. Cambridge University Press, Cambridge, United

13 Kingdom and New York, NY, USA.

14 Deser, C., Phillips, A., Bourdette, V. & Teng, H., 2012a: Uncertainty in climate change

15 projections: the role of internal variability. *Clim. Dynam.* 38, 527–547.

16 Deser, C., R. Knutti, S. Solomon, & A. S. Phillips, 2012b: Communication of the role of

17 natural variability in future North American climate. *Nat. Clim. Change*, 2, 775-779,

18 doi: 10.1038/nclimate1562.

19 Deser, C., A. S. Phillips, M. A. Alexander & B. V. Smoliak, 2014:. Projecting North

20 American Climate over the next 50 years: Uncertainty due to internal variability. *J.*

21 *Climate*, 27, 2271-2296.

22 Feldstein, S. B., 2000: Teleconnections and ENSO: The timescale, power spectra, and

23 climate noise properties. *J. Climate*, 13, 4430.

24 Fischer, E. & Schär, C, 2009: Future changes in daily summer temperature variability:

1 driving processes and role for temperature extremes. *Clim. Dynam.* 33, 917–935.

2 Gregory, J. M. & Mitchell, J. F. B., 1995: Simulation of daily variability of surface
3 temperature and precipitation over Europe in the current and 2xCO₂ climates using
4 the UKMO high-resolution climate model. *Q. J. R. Meteorol. Soc.*, 121, 1451-1476.

5 Hartmann, D. L. & Lo, F., 1998: Wave-driven zonal flow vacillation in the Southern
6 Hemisphere. *J. Atmos. Sci.*, 55, 1303–1315.

7 Hawkins, E. & Sutton, R., 2009: The potential to narrow uncertainty in regional climate
8 predictions. *Bull. Amer. Meteor. Soc.*, 90, 1095–1107.

9 Hawkins, E. & Sutton, R., 2011: The potential to narrow uncertainty in projections
10 of regional precipitation change. *Clim. Dynam.* 37, 407–418.

11 Held, I. M. & Soden, B. J., 2006: Robust Responses of the Hydrological Cycle to Global
12 Warming. *J. Climate*, 19, 5686–5699.

13 IPCC, 2014: Summary for policymakers. In: *Climate Change 2014: Impacts, Adaptation,*
14 *and Vulnerability. Part A: Global and Sectoral Aspects. Contribution of Working*
15 *Group II to the Fifth Assessment Report of the Intergovernmental Panel on Climate*
16 *Change [Field, C.B., et al. (eds.)]. Cambridge University Press, Cambridge, United*
17 *Kingdom and New York, NY, USA, pp. 1-32.*

18 Kay, J. E., et al. The Community Earth System Model (CESM) Large Ensemble Project:
19 A Community Resource for Studying Climate Change in the Presence of Internal
20 Climate Variability. *Bull. Amer. Met. Soc.*, in press.

21 Kennedy J.J., Rayner, N.A., Smith, R.O., Saunby, M. and Parker, D.E., 2011:
22 Reassessing biases and other uncertainties in sea-surface temperature observations
23 measured in situ since 1850 part 2: biases and homogenisation. *Journal of*
24 *Geophysical Research* 116, D14104, doi:10.1029/2010JD015220.

1 Kirtman, B., S.B. Power, et al., 2013: Near-term Climate Change: Projections and
2 Predictability. In: Climate Change 2013: The Physical Science Basis. Contribution of
3 Working Group I to the Fifth Assessment Report of the IPCC [Stocker, T.F., et al.
4 (eds.)]. Cambridge University Press, Cambridge, United Kingdom and New York,
5 NY, USA.

6 Knutson, T. R., F. Zeng, & A. T. Wittenberg, 2013: Multimodel Assessment of Regional
7 Surface Temperature Trends: CMIP3 and CMIP5 Twentieth-Century Simulations,
8 26, 8709-8743.

9 Mitchell, J. M., Jr., B. Dzerdzeevskii, H. Flohn, W. L. Hofmeyr, H. H. Lamb, K. N. Rao &
10 C. C. Wallen, 1966: Climatic Change, Techn. Note 79, 79 pp., World Meteorol. Org.,
11 Geneva.

12 Newman, M., Compo G. P., & Alexander M. A., 2003: ENSO-forced variability of the
13 Pacific decadal oscillation. *J. Climate*, 23, 3853-3857.

14 Osborn, T.J. and Jones, P.D., 2014: The CRUTEM4 land-surface air temperature data
15 set: construction, previous versions and dissemination via Google Earth. *Earth
16 System Science Data* 6, 61-68, doi:10.5194/essd-6-61-2014.

17 Santer, B. D., T. M. L. Wigley, J. S. Boyle, D. J. Gaffen, J. J. Hnilo, D. Nychka, D. E.
18 Parker & K. E. Taylor, 2000: Statistical significance of trends and trend differences
19 in layer average atmospheric temperature time series, *J. Geophys. Res.*, 105, 7337–
20 7356.

21 Schneider, T., T. Bischoff, and H. Plotka, 2015: Physics of changes in synoptic
22 midlatitude temperature variability. *Journal of Climate*, submitted.

23 Screen J. A., 2014: Arctic amplification decreases temperature variance in Northern
24 mid- to high-latitudes, *Nature Climate Change*, DOI:10.1038/nclimate2268.

- 1 von Storch, H. & Zwiers, F. W., 1999: Statistical Analysis in Climate Research
2 Cambridge University Press, 484 pp.
- 3 Wallace, J. M., Y. Zhang & J. A. Renwick, 1995: Dynamic contribution to hemispheric
4 mean temperature trends, *Science*, 270, 780-783.
- 5 Wallace, J. M., Q. Fu, B. V. Smoliak, P. Lin & C. M. Johanson, 2012: Simulated versus
6 observed patterns of warming over the extratropical Northern Hemisphere
7 continents during the cold season. *Proc. Natl. Acad. Sci.*, 109, 14332-14337.
- 8 Wallace, J.M. C. Deser, B.V. Smoliak, & A.S. Phillips, 2013: Attribution of climate
9 change in the presence of internal variability, In *Climate Change: Multidecadal and*
10 *Beyond* (Eds: C.P. Chang, M. Ghil, M. Latif, and J. M. Wallace). World Scientific
11 Series on Asia-Pacific Weather and Climate, Vol. 6.
- 12 Zhang, C., 2005: Madden-Julian Oscillation. *Rev. Geophys*, 43, RG2003, Wilks, D. S.,
13 1995: *Statistical Methods in the Atmospheric Sciences: An Introduction*. Academic
14 Press, 467 pp.

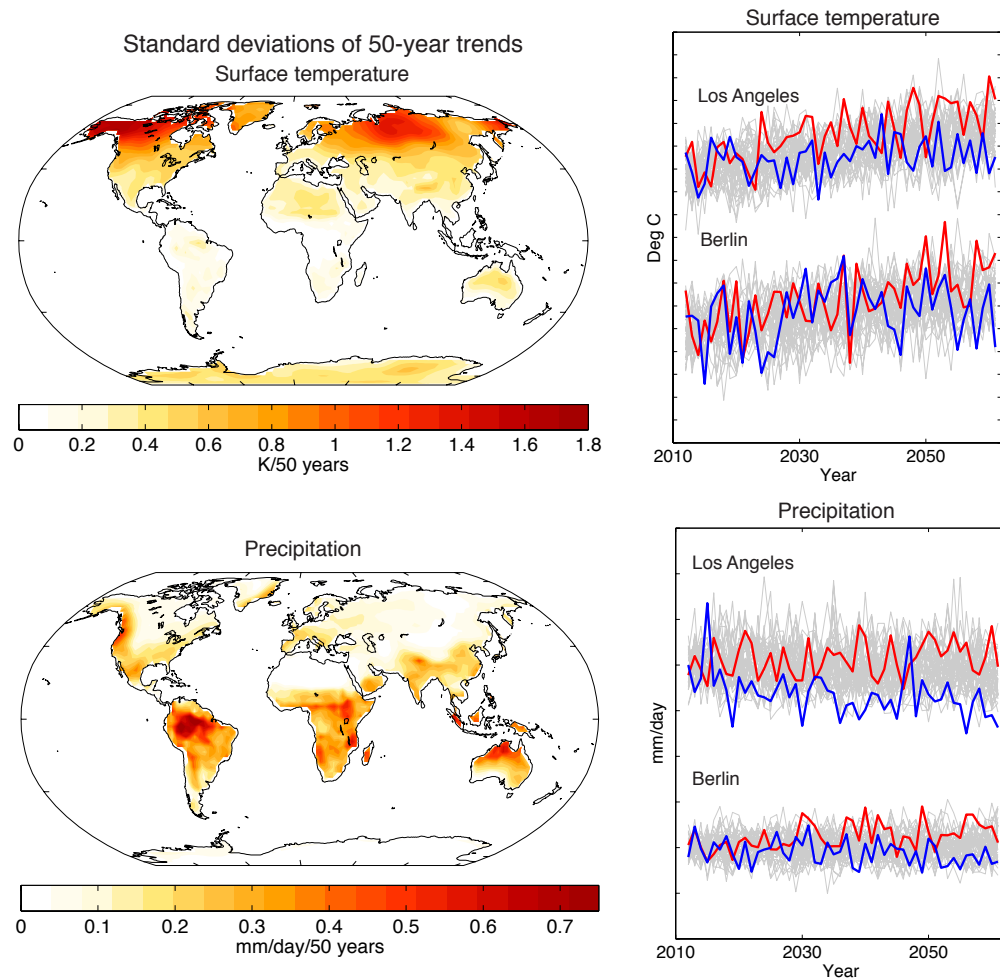


Figure 1. Left. The standard deviations of the 50 year trends in October-March mean surface temperature (top) and precipitation (bottom) based on output from the NCAR 40-member ensemble of climate change simulations. Trends are expressed as the total change over the 50 year period 2011-2061. The trend standard deviations indicate the spread in the trends derived from all 40 ensemble members. **Right.** Wintertime mean time series of surface temperature (top) and precipitation (bottom) for indicated locations. The grey lines show results for all 40 ensemble members; the red and blue lines indicate the ensemble members with the largest and smallest trends over the 2011-2061 period, respectively. Tickmarks at 1 deg C and 1 mm/day.

Trend amplitude required to exceed the 95% margin of error
(relative to the standard deviation of the internal variability)

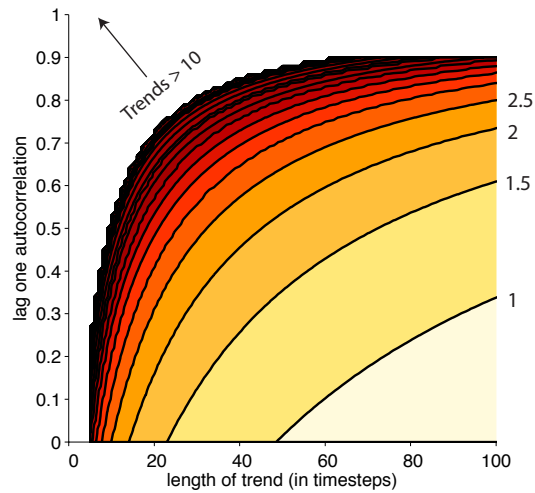


Figure 2. Analytic solutions for the uncertainty in future climate due to internal variability. Trend amplitude required to exceed the 95% margin of error relative to the standard deviation of the internal variability. For example, a trend of “2” indicates that the trend must be twice as large as the internal (unforced) variability to exceed the 95% margin of error. Results are derived from Equation 8 and are shown as a function of the trend length (in timesteps) and the lag-one autocorrelation (r_1). Contours are spaced at trend amplitudes of 0.5.

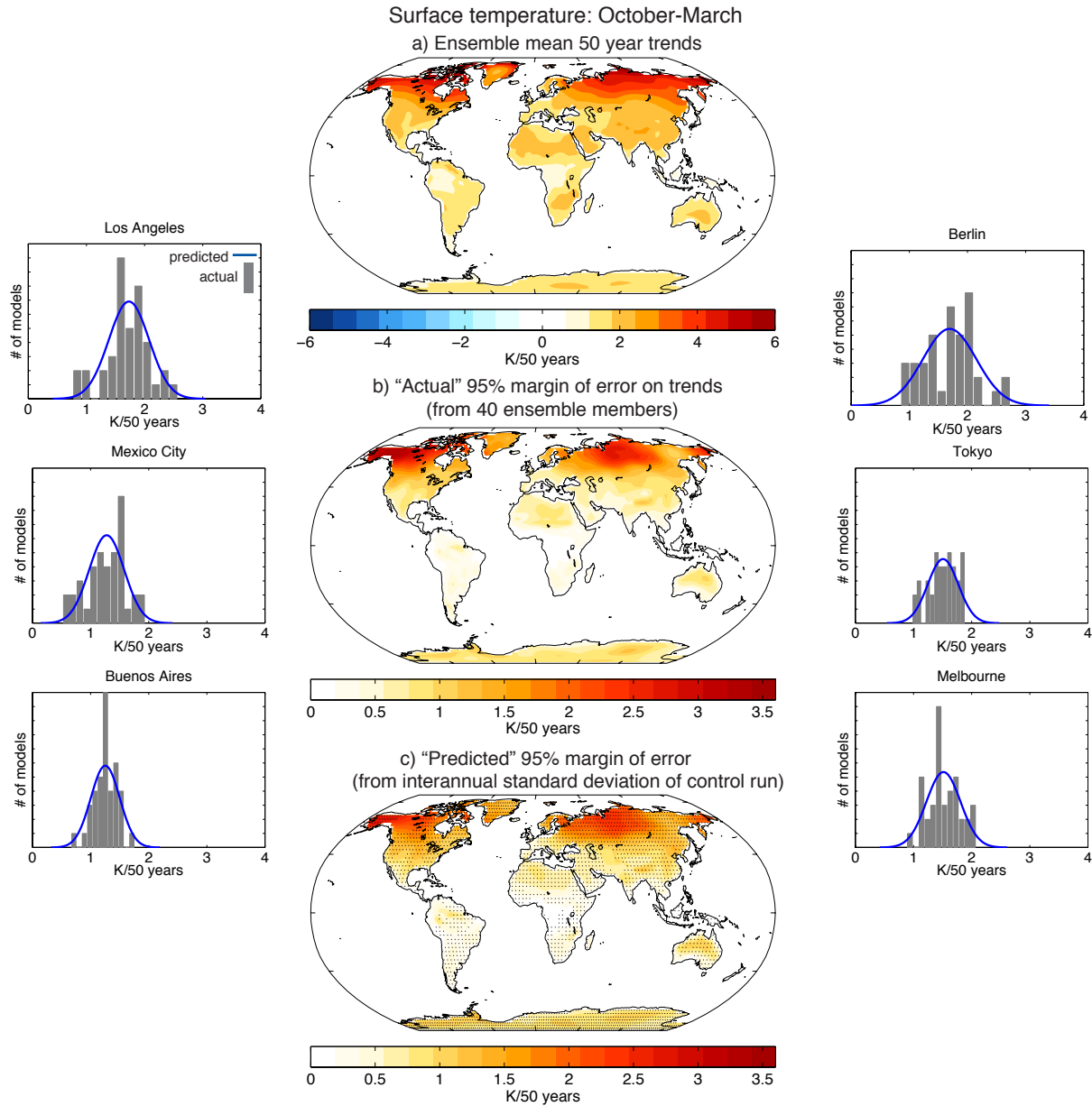


Figure 3. Using the control run to estimate the 95% margins of error on 50-year trends in October-March mean surface temperature. **a)** The “forced response” defined as the linear trends in October-March mean surface temperature averaged over all 40 ensemble members in $K/50$ years. **b)** The “actual” 95% margins of error on the 50 year trends derived from all 40 ensemble members. **c)** The “predicted” 95% margins of error on the 50 year trends derived from the control run interannual standard deviations (as per Eq. 10). Stippling indicates regions where the predicted margins are within the 95% confidence limits on the actual margins shown in panel b), based on a test of the Chi-squared distribution with 40 independent samples (**Surrounding panels**) The probability distribution functions of the 50 year trends at grid boxes corresponding to the indicated cities. Grey bars denote the histograms derived from all 40 ensemble members; the blue curves the distribution functions predicted by the interannual standard deviations from the control run. The areas under the blue curves are normalized so that they match the areas under the attendant gray bars.

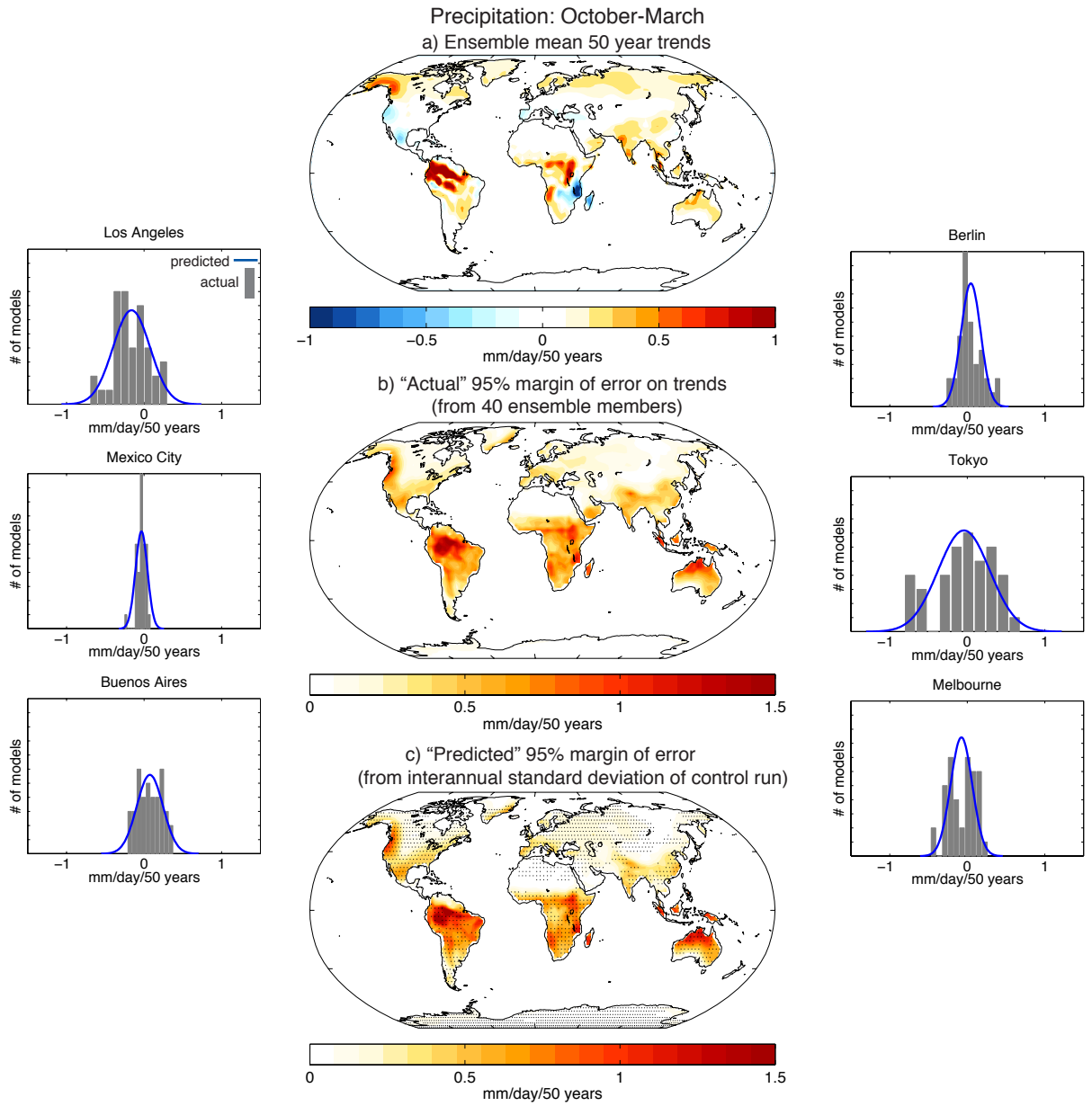


Figure 4. As in Fig. 3, except for October-March mean precipitation. Trends are expressed in mm/day/50 years.

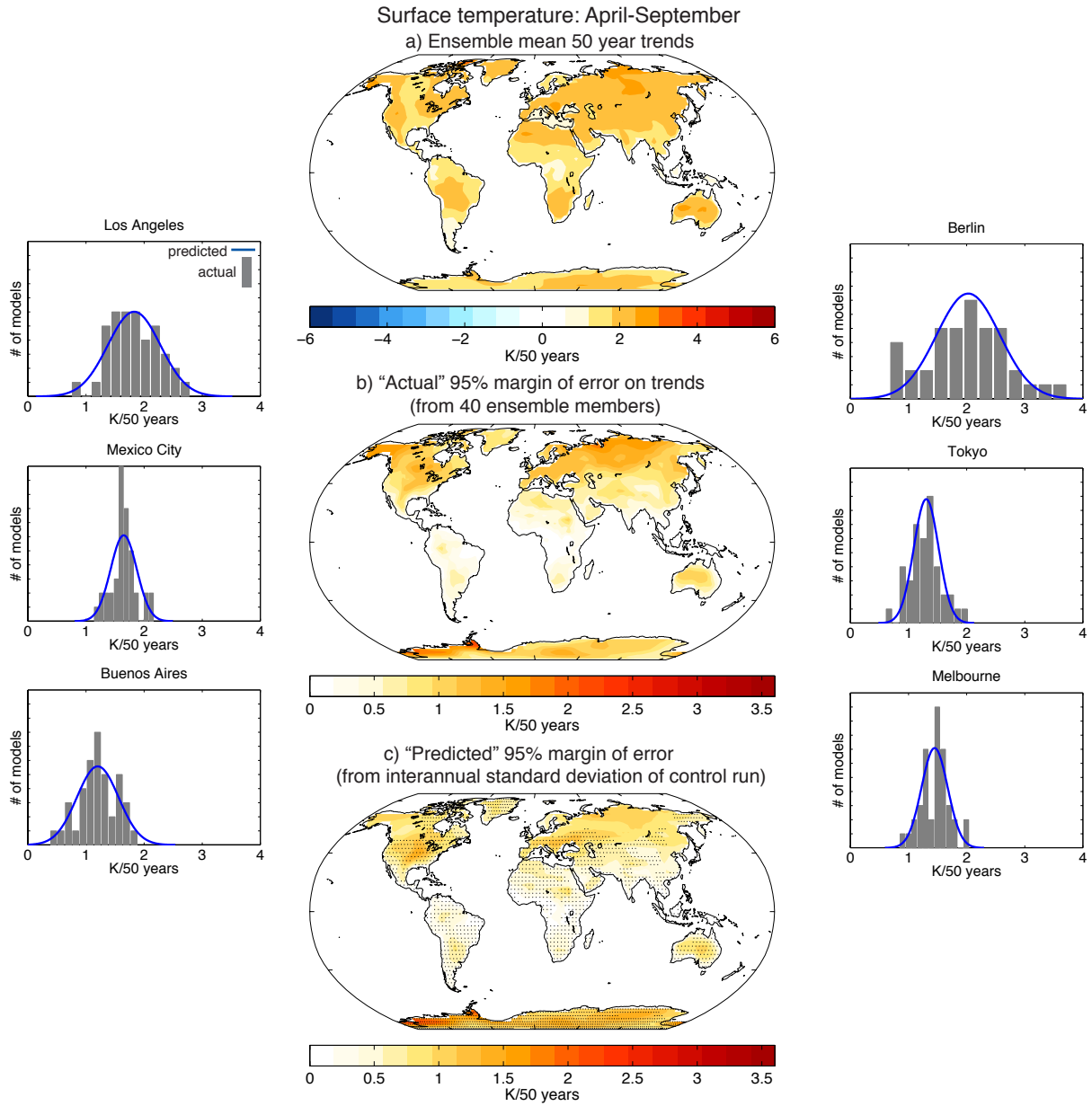


Figure 5. As in Fig. 3, except for April-September mean surface temperature.

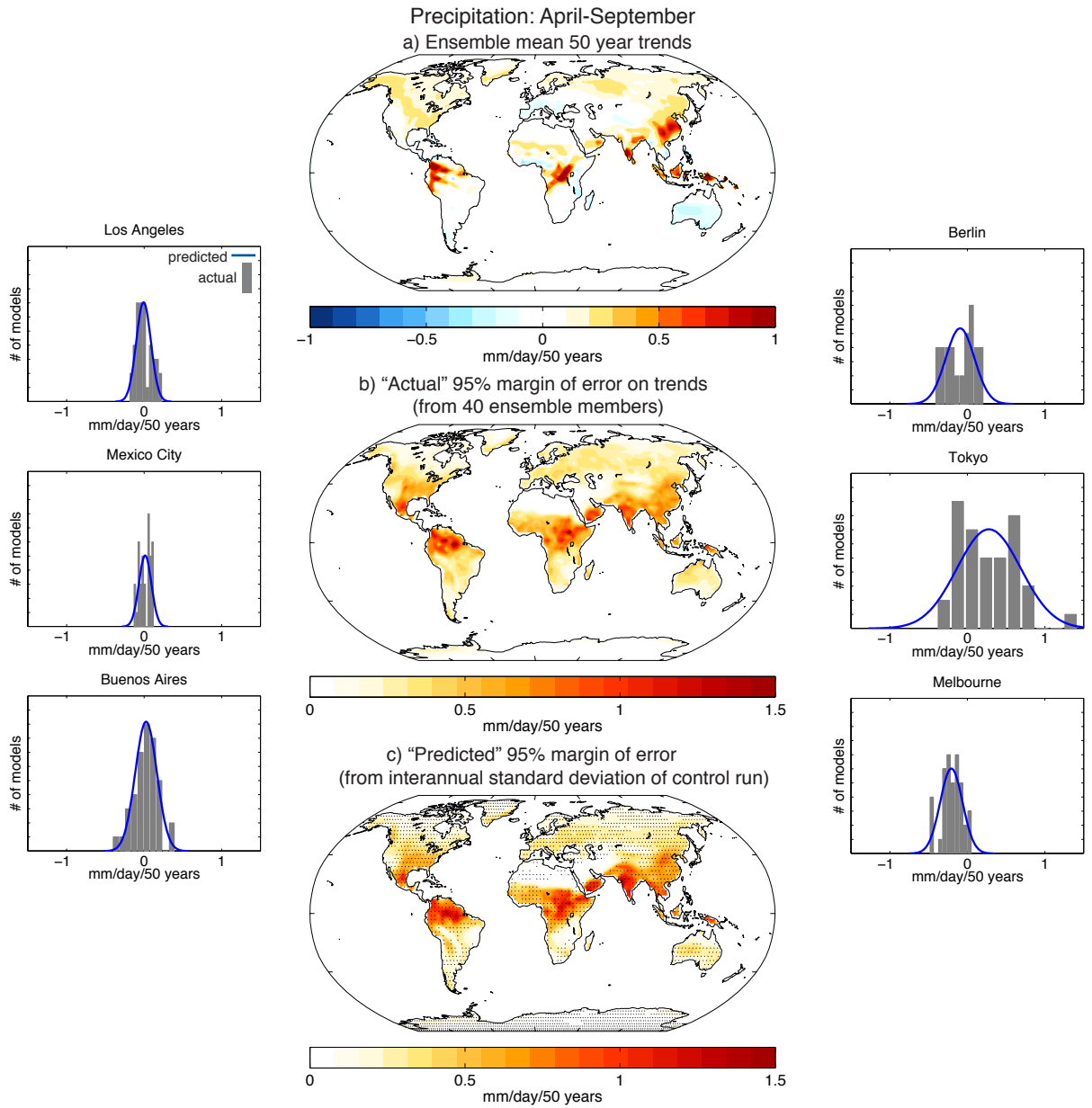


Figure 6. As in Fig. 3, except for April-September mean precipitation.

Surface temperature: April-September

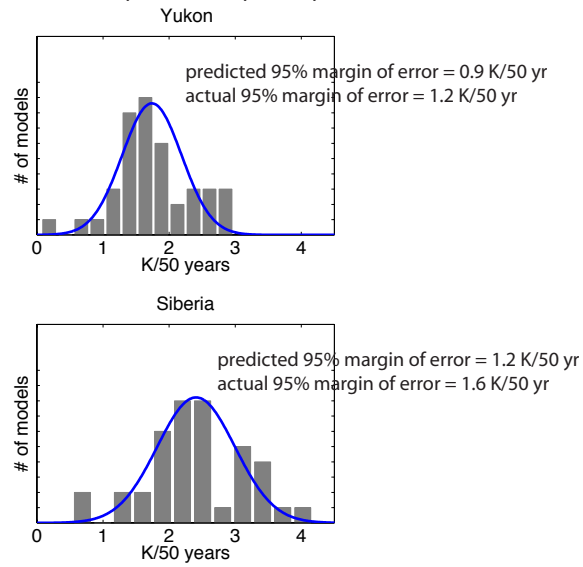


Figure 7. As in the probability distribution functions/histograms in Fig. 5, but for April-September mean temperature trends averaged over the Yukon (60N; 240E) and Siberia (65N; 90E). The predicted and actual 95% margins of error on the trends are indicated on the figure.

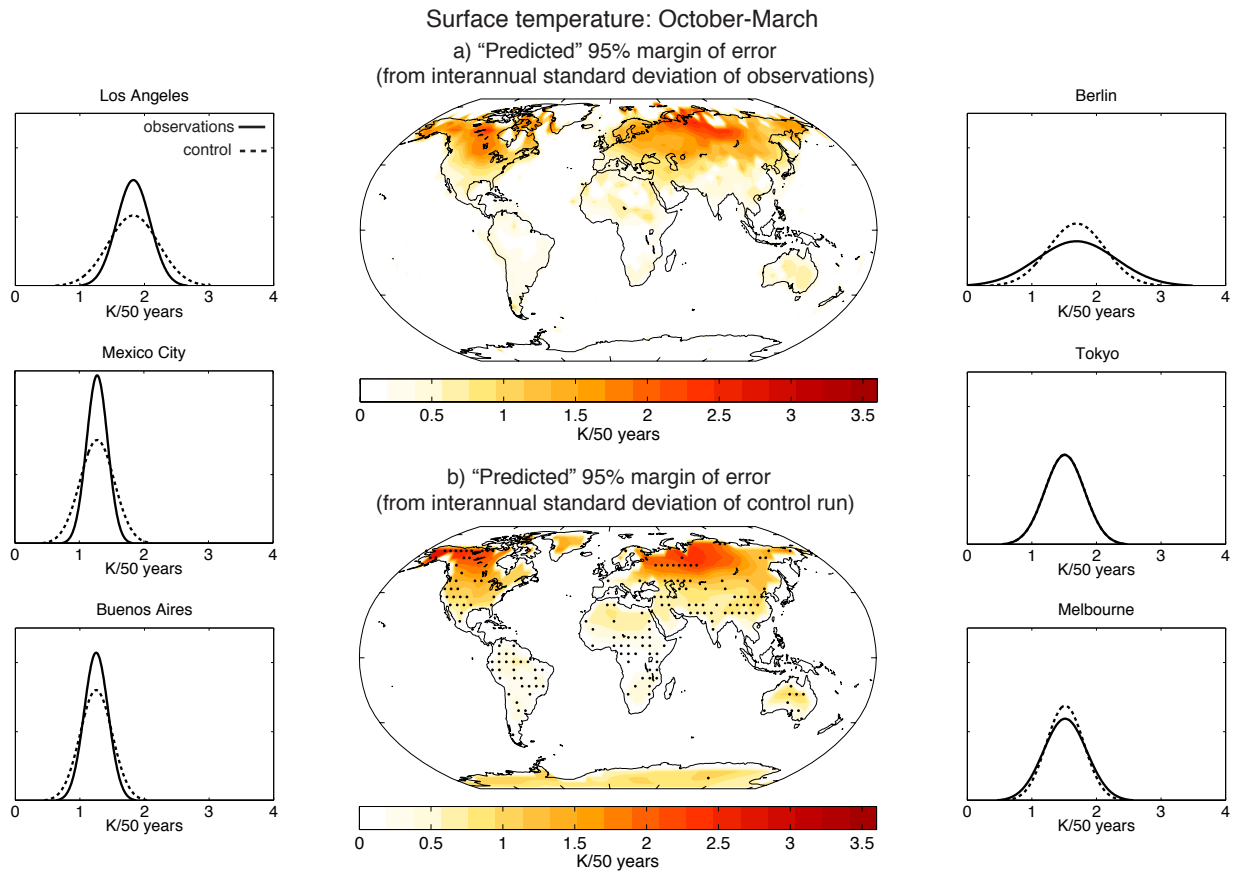


Figure 8. Using observations to estimate the 95% margins of error on 50-year trends in October-March mean surface temperature. **(top)** The “predicted” 95% margins of error on the 50 year trends derived from the observed interannual standard deviations (as per Eq. 10). **(bottom)** The “predicted” 95% margins of error derived from the control run interannual standard deviations. The bottom panel is the same as that shown in Fig. 2c except that 1) the stippling indicates regions where the modeled and observed margins of error are significantly different from each other at the 95% confidence level; and 2) the model output has been interpolated to the same mesh as the observations. See text for details. **(Surrounding panels)** The probability distribution functions of the 50 year trends at grid boxes corresponding to the indicated cities. Solid and dashed curves denote the distribution functions predicted by the interannual standard deviations of the observations and the interpolated control simulation output, respectively. Distributions are normalized so that they have the same area.

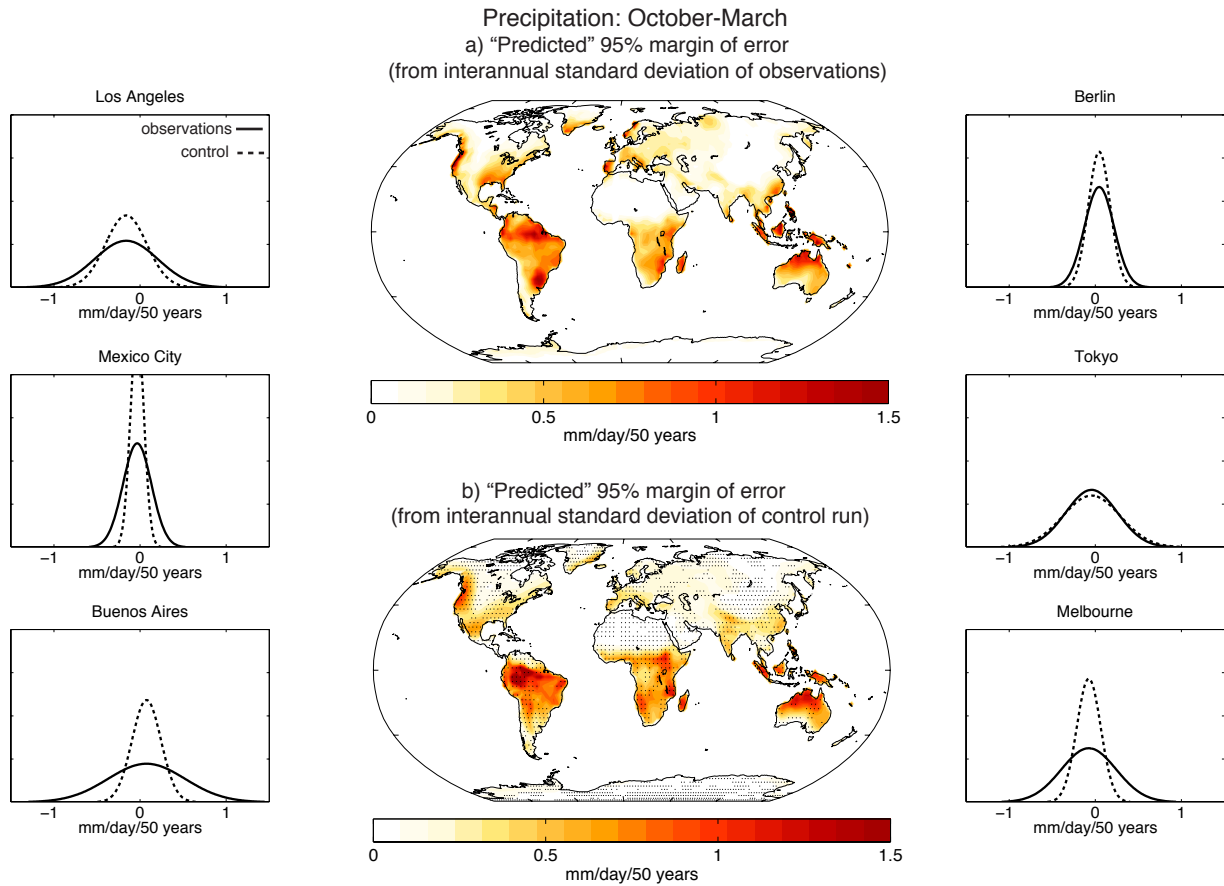
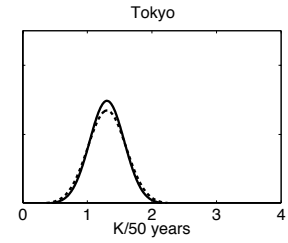
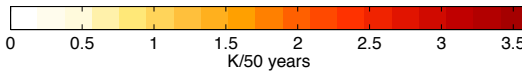
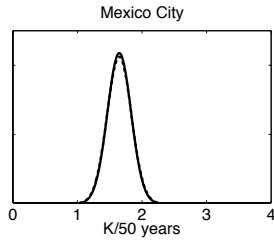
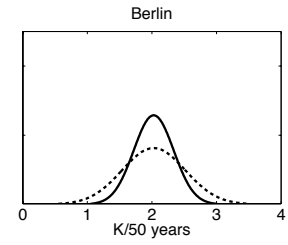
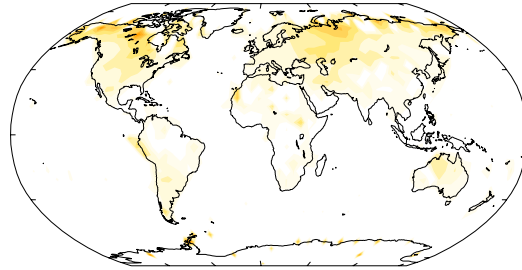
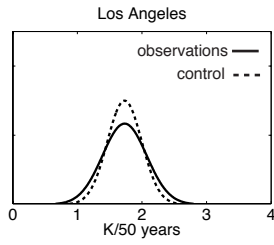


Figure 9. As in Fig. 8, but for October-March mean precipitation. The observations have been interpolated to the same mesh as the model output.

Surface temperature: April-September
a) "Predicted" 95% margin of error
(from interannual standard deviation of observations)



b) "Predicted" 95% margin of error
(from interannual standard deviation of control run)

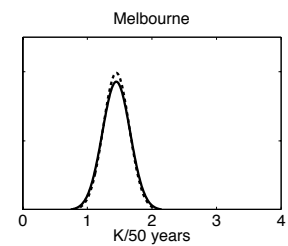
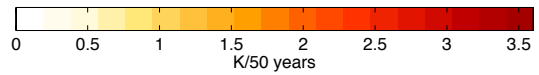
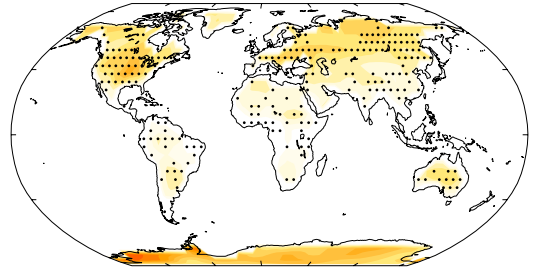
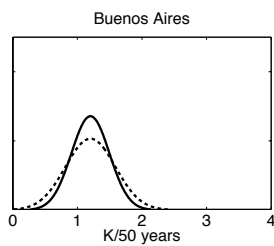


Figure 10. As in Fig. 8, but for April-September mean temperature.

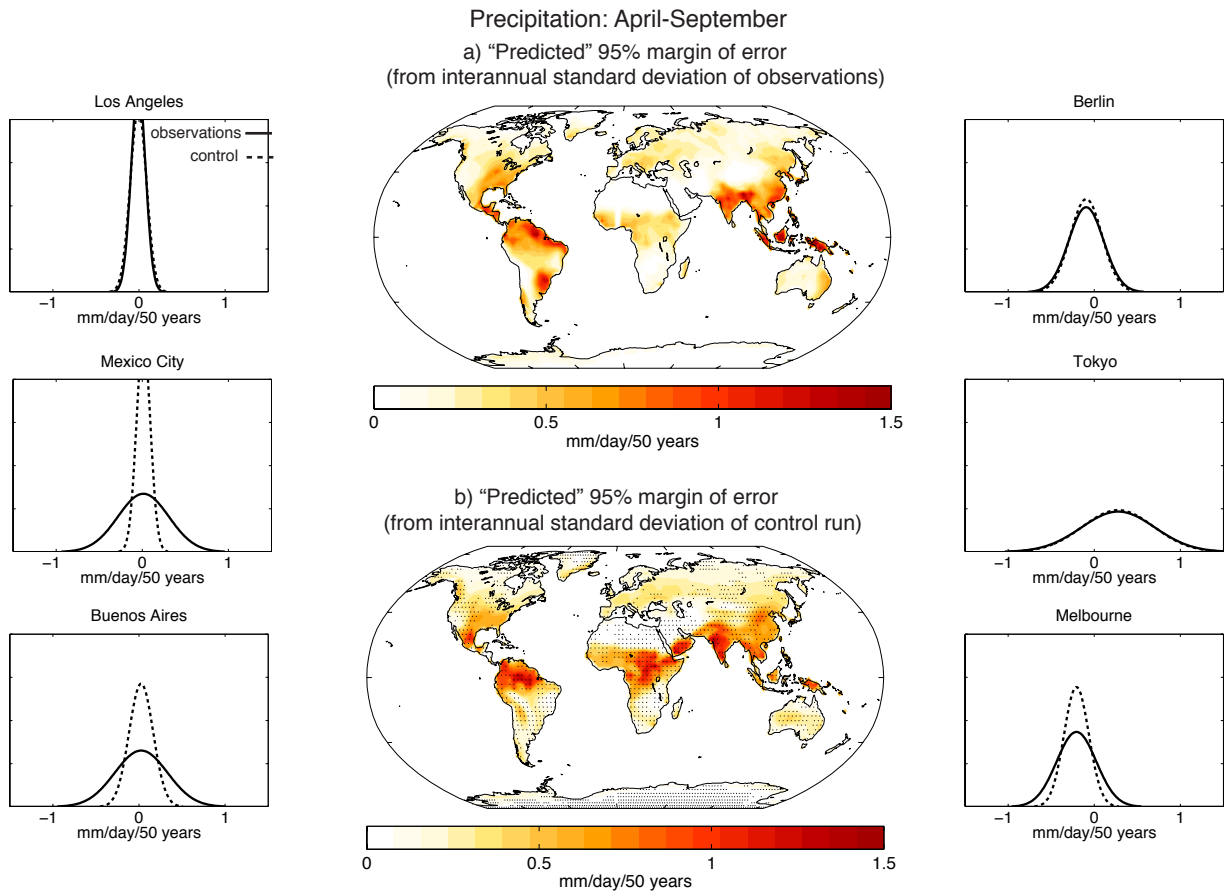
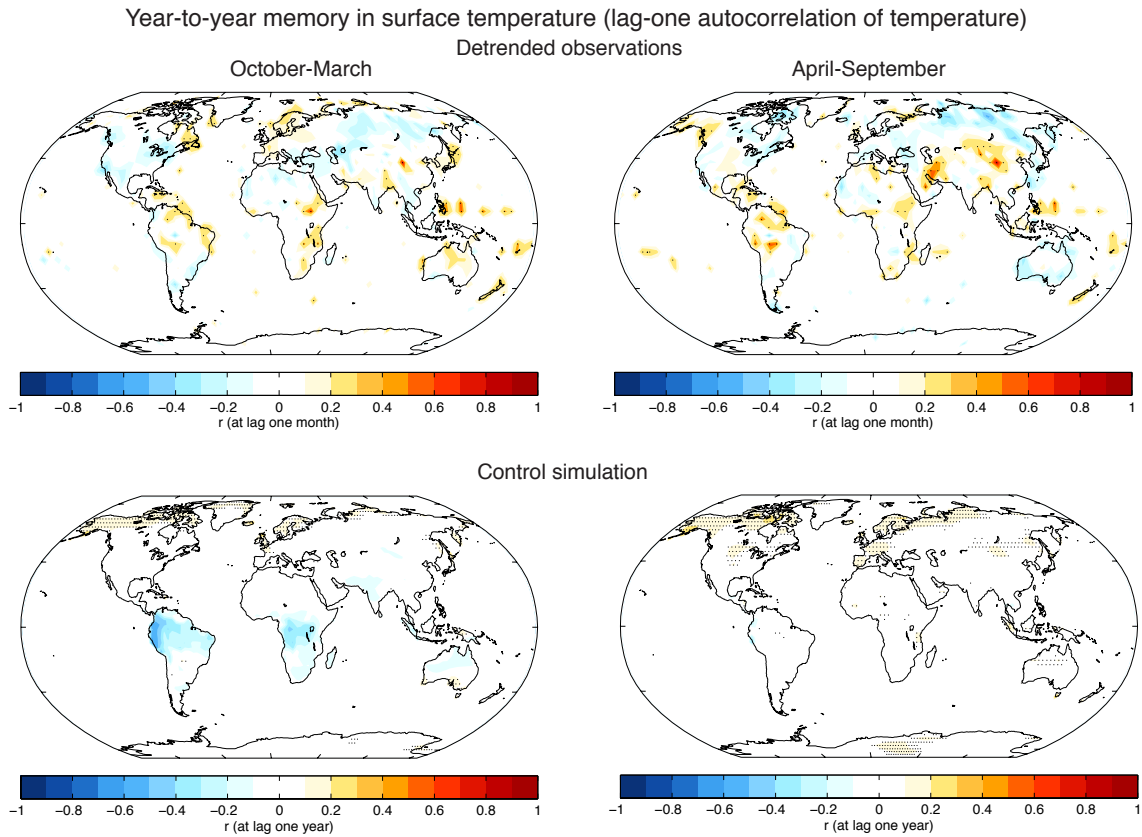
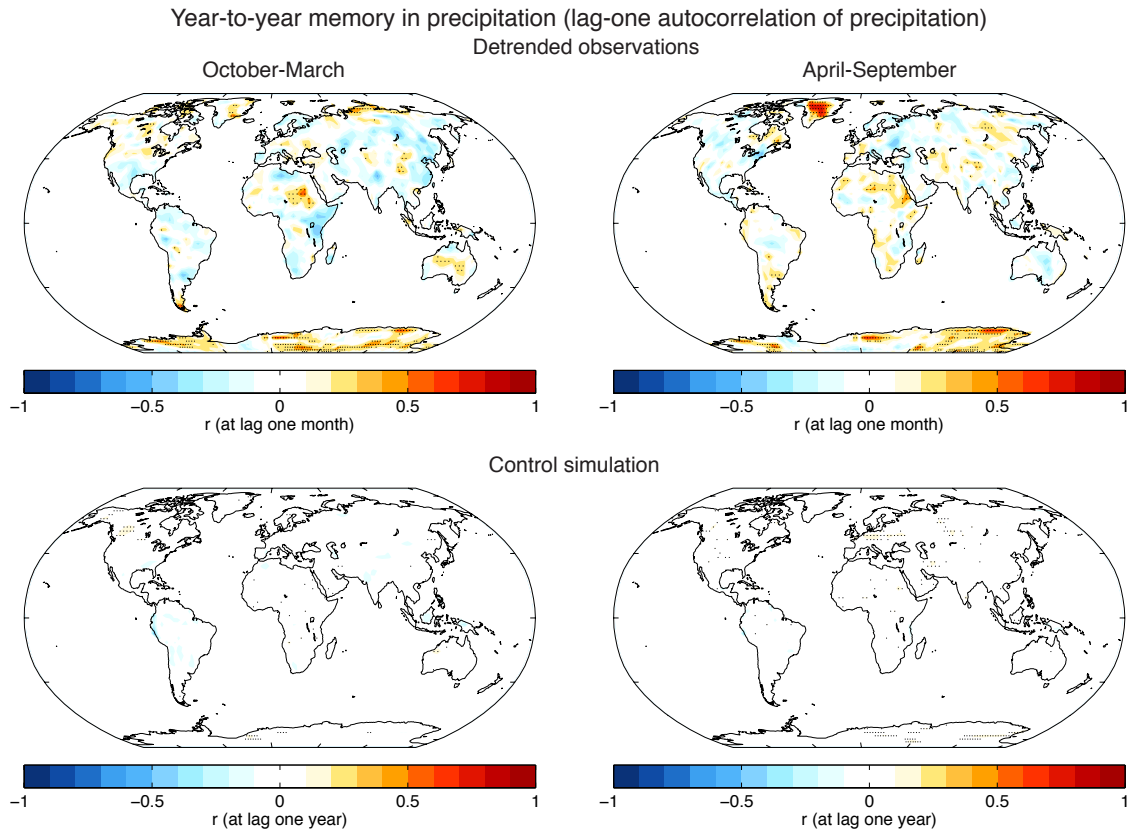


Figure 11. As in Fig. 8, but for April-September mean precipitation.

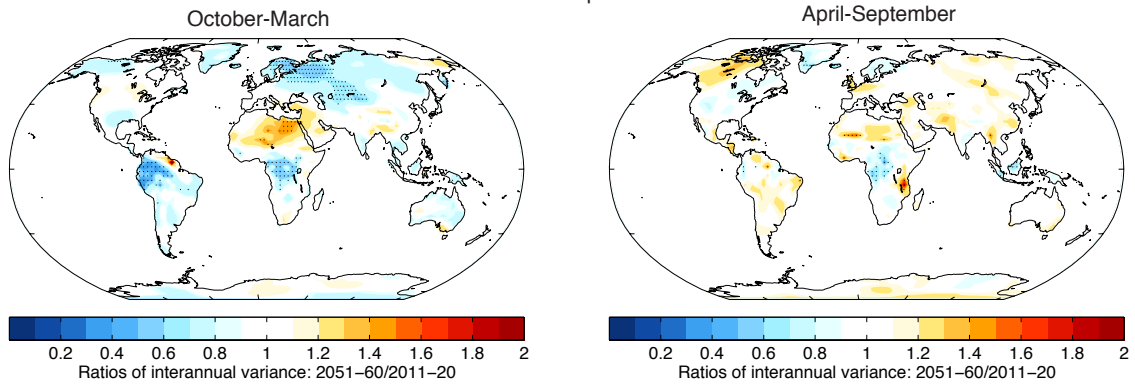


Appendix Figure A1. Autocorrelations of seasonal-mean surface temperature based on detrended observations 1979-2013 (top) and 500-years of control simulation output (bottom). Stippling indicates regions where the autocorrelations are significant at the 95% level based on a one-tailed test of the t-statistic with 500 (control simulation) and 35 (observations) independent samples.

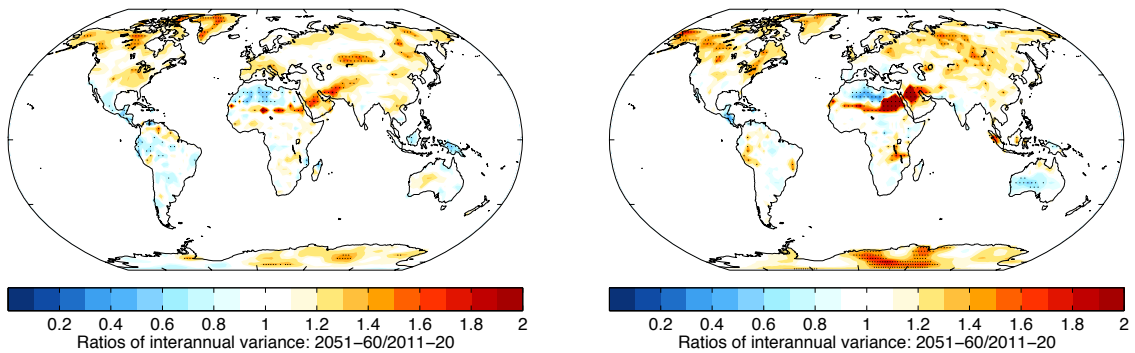


Appendix Figure A2. As in Fig. A1, but for seasonal-mean precipitation.

Ratio of variances of interannual variability between 2051-2060 and 2011-2020
Surface temperature



Precipitation



Appendix Figure A3. Ratio of variances between the periods 2051-2060 and 2011-2020 from the NCAR 40-member ensemble of climate change simulations. The variances are calculated as the pooled detrended seasonal-mean data from all ensemble members. Ratios greater than ~ 1.4 and less than ~ 0.71 (indicated by stippling) are significant at the 95% level based on the F-statistic.